Supporting Information

How Well Can We Predict Cluster Fragmentation Inside a Mass Spectrometer?

Monica Passananti,[a,b] *Evgeni Zapadinsky,*[a] *Tommaso Zanca,*[a] *Juha Kangasluoma,*[a,c] *Nanna Myllys,*[a,d] *Matti P. Rissanen,*[a] *Theo Kurtén,*[e] *Mikael Ehn,*[a] *Michel Attoui* [f] *and Hanna Vehkamäki* [a]

[a] Institute for Atmospheric and Earth System Research / Physics, Faculty of Science, University of Helsinki, Finland

[b] Present address: Dipartimento di Chimica, Università di Torino, Via Giuria 5, 10125 Torino, Italy.

[c] Aerosol and Haze Laboratory, Beijing Advanced Innovation Center for Soft Matter Science and Engineering, Beijing University of Chemical Technology, 100029 Beijing, China

[d] Present address: Department of Chemistry, University of California, Irvine, California 92697-2025, United States

[e] Institute for Atmospheric and Earth System Research / Chemistry, Faculty of Science, University of Helsinki, Finland

[f] LISA, University Paris Est Creteil, Creteil, 94010, France

Corresponding Author

***** E-mail: monica.passananti@helsinki.fi

Table of Contents

1. Chemicals

All chemicals were used without further purification: sulfuric acid (H_2SO_4) (95-97%), Terephthalic acid (98%), malonic acid (99%), 1-Ethyl-3-methylimidazolium bis(trifluoromethylsulfonyl)imide (EMIM BTI) (>98%), 1-Ethyl-3-methylimidazolium dibutyl phosphate (EMIM DBP) (>97%) and tetraheptylammonium bromide (THAB) (>99%) were obtained from Sigma Aldrich. Solutions are prepared with methanol HPLC fluorescence grade (purchased from Fisher Chemical) and deionized ultra-pure aerated Milli-Q water from Millipore.

2. Experimental set-up

The experiments were carried out using an ElectroSpray Ionization Differential Mobility Analyser Atmospheric Pressure interface Time Of Flight mass spectrometer (ESI-DMA-APi-TOF). A schematic representation of the experimental set-up can be found in the main text (Figure 1).

A solution of sulfuric acid 200 mM in water/methanol 1/1 v/v was used to generate negatively charged sulfuric acid clusters by ESI. The electrospray was generated applying a negative voltage to the solution and a positive pressure was used to drive the solution through the silica capillary (30 μm tip i.d., 360 μm o.d., non-coated, SilicaTip™, PicoTip™ EMITTER, NewObjective). We decided to work in negative mode because sulfuric acid is usually detected with nitrate-CI-APi-TOF in negative mode.[1] The generated charged clusters were separated with a high resolution Herrmann-type DMA operating with a flow of 10 L/min, a description of the DMA is published elsewhere.[2] The DMA mobility classification was calibrated before each experiment with THAB positive monomer. The resolution was calculated from the THAB positive monomer peak, and it is defined as the ratio of the DMA voltage at the maximum of the peak and full width at half maximum (FWHM). Using a Gaussian fit to calculate the FWHM a resolution of 19.7 was obtained. To the DMA was connected a TSI aerosol electrometer (model 3068B) with an inlet flow rate of 5 L/min and the APi-TOF with an inlet flow rate of 0.8 L/min. The APi-TOF (Tofwerk AG, Thun, Switzerland) consists of an atmospheric pressure interface (APi), made by three vacuum chambers, coupled with a time-of-flight mass spectrometer. The pressure decreases between successive chambers until reducing to 10^{-6} mbar at the time of flight mass spectrometer. In the first two chambers the ions are guided through quadrupoles (Q1 and Q2), while in the last chamber (3rd chamber) several lenses focus the ions. In total, 27 voltages and 2 radio frequencies are applied to the APi-TOF, most of which can be changed to optimize the results as a function of the specific application of the instrument. A more detailed description of the instrument is reported elsewhere.[3] The APi-TOF was operated in negative mode and the data were analysed using a Matlab-based set of programs (tofTools) developed at the University of Helsinki.

3. Fragmentation experiments and transmission measurement

We chose one voltage configuration with a relatively low fragmentation fraction (30% of $(SA)_3^-$ fragmentation) and a relatively high signal-to-noise ratio (SNR = 80 for $(SA)_3^-$ averaging time 30 seconds) as our standard configuration. The fragmentation experiments were carried out by changing, one at a time, all the voltages applied to the atmospheric pressure interface (APi), in total 13 voltages, without changing the radiofrequencies. A schematic representation of the APi is reported in Figure S1. Only the Deflector and Deflector Flange were changed together because they are used to orient the ion beam. We calculated the percentage ratio of sulfuric acid monomer ($R_{(SA)_1^-}$), dimer ($R_{(SA)_2^-}$) and trimer ($R_{(SA)_3^-}$) using the following formula:

$$R_{(SA)_i^-} = \frac{(SA)_i^-}{\sum_{i=1}^{N}(SA)_i^-} \times 100 \qquad \text{eq.1}$$

with N=3.

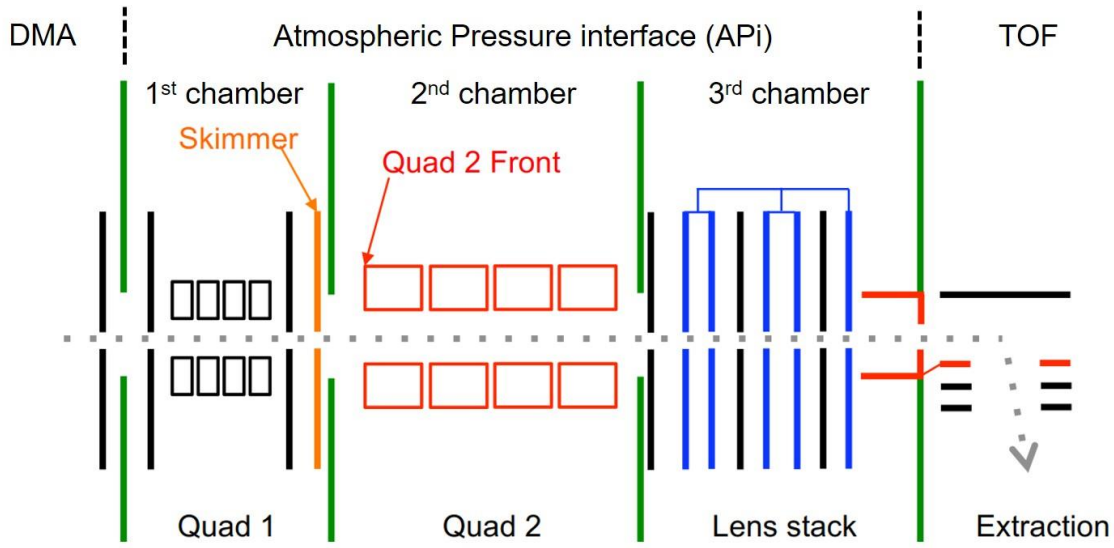

Figure S1. A schematic of the voltages in the APi region of the Tofwerk ToF-MS (modified from Lopez-Hilfiker et al. 2016).[4]

The fragmentation was measured for 76 different voltage configurations. It is important to note that the range of voltages applied to these electrodes were large, in some cases the applied voltage was 100 V lower or 80 V higher than in the standard configuration.

The voltage configuration of the instrument can affect not only the fragmentation of clusters but also the mass-dependent transmission efficiency.[5] To verify that the observed change in the ratio between $(SA)_2^-$ and $(SA)_3^-$ is due to fragmentation, and not to transmission changes, we measured the relative ion transmission for the size region of $(SA)_1^-$, $(SA)_2^-$ and $(SA)_3^-$, for a set of representative configurations (24 voltage configurations). The transmission (T) of the APi-TOF is defined as the fraction of ions reaching the detector out of the ions reaching the inlet, and it takes into account the ion losses from the inlet until the detector. It strongly depends on the voltage configuration of the instrument and it is a mass-dependent.[3, 5] This means that small ions (low masses) may have higher transmission compared to large ions (high masses) for some voltage configurations, and the opposite for some other configurations. The transmission can be measured by selecting a mono-mobile ion size distribution from the DMA, and comparing the counts in the APi-TOF to those of the electrometer. The electrometer and the inlet of the APi-TOF (Nozzle) were equidistant from the exit of the DMA, therefore we considered that the ion losses in these regions are equivalent. Four different molecular ions (produced by ionizing molecules or ionic liquids) were used for the transmission measurement, these ions are very unlikely to fragment in the instrument due to their chemical structure. They were produced by spraying malonic acid, terephthalic acid, EMIM BTI and EMIM DBP in the negative mode. The ion monomer of each molecule was selected with the DMA. The mass of these ions cover the mass range of interest (from around 100m/z to 300m/z). While the absolute transmission for different voltage configurations was quite different (see Figure S2), the differences between the relative transmissions of $(SA)_1^-$, $(SA)_2^-$ and $(SA)_3^-$ were small. The signal intensity (ions/second) of sulfuric acid monomer, dimer and trimer was recalculated according to the ion transmission. The transmission correction changes the ratio between $(SA)_2^-$ and $(SA)_3^-$ only by

approximately 5%. The highest change in the $R_{(SA)_3^-}$ due to the transmission correction was of 14.6% and in average a 7.6% of change was observed due to the transmission change. The effect of the mass-dependent transmission efficiency is small mainly because the mass range of interest is relatively small (less than 100 m/z difference between sulfuric acid dimer and trimer),[3] and we did not change the settings that have a significant impact on the mass-dependent transmission efficiency, namely radiofrequencies and radiofrequencies amplitude voltages applied to the quadrupoles (Q1 and Q2), and voltages applied in the TOF.[5]

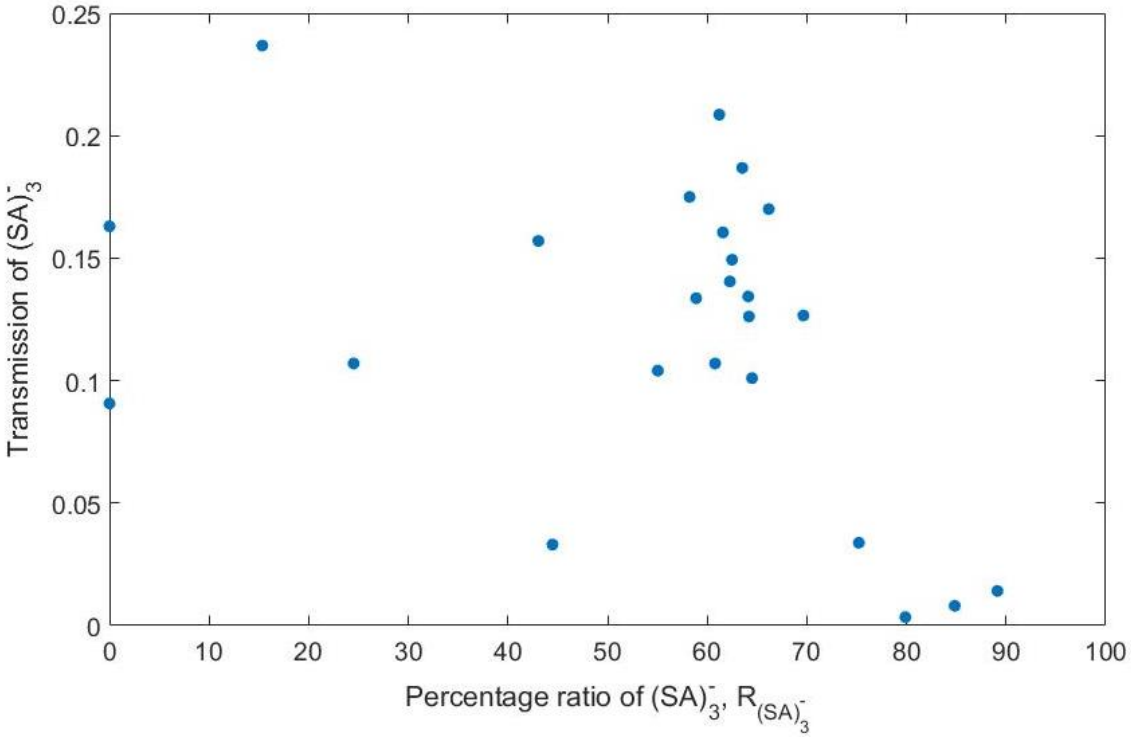

Figure S2. Absolute transmission of $(SA)_3^-$ as a function of percentage ratio of surviving sulfuric acid trimer negatively charged ($R_{(SA)_3^-}$).

The percentage ratio between the signal of sulfuric acid monomer, dimer and trimer in all tested conditions are reported in Figure S3 to Figure S14, and for the cases where transmission has been measured, the data corrected by transmission changes are also shown in the figures. When no bar is

reported for a specific voltage value, it means that for the corresponding voltage configuration the ion transmission was zero and no ions reached the detector. This was the case for 8 conditions (voltage configurations).

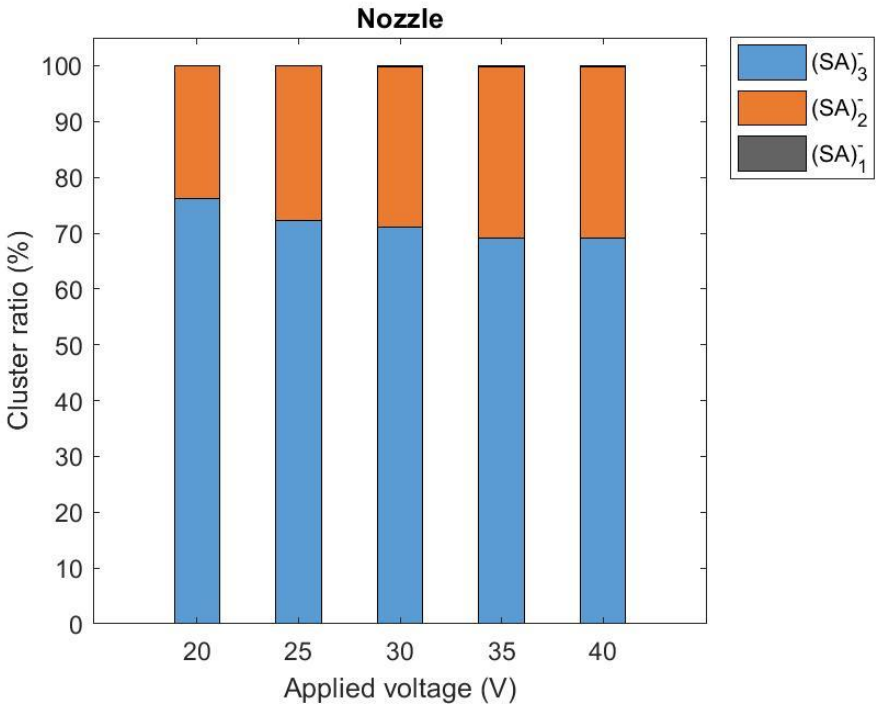

Figure S3. Percentage ratio of $(SA)_1^-$, $(SA)_2^-$ and $(SA)_3^-$ for different voltages applied to Nozzle.

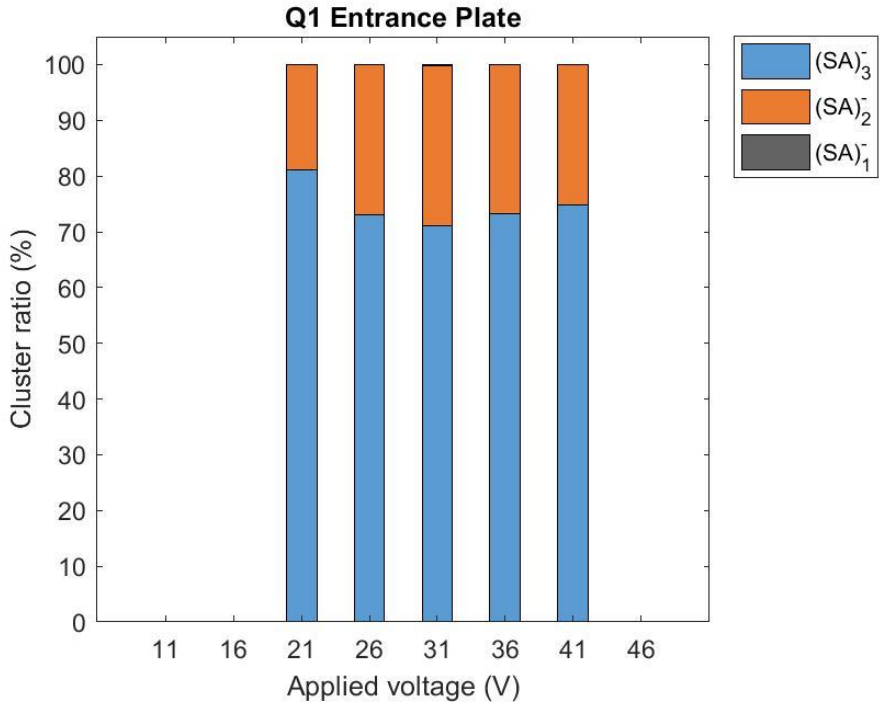

Figure S4. Percentage ratio of $(SA)_1^-$, $(SA)_2^-$ and $(SA)_3^-$ for different voltages applied to Q1 Entrance Plate (Q1 EP).

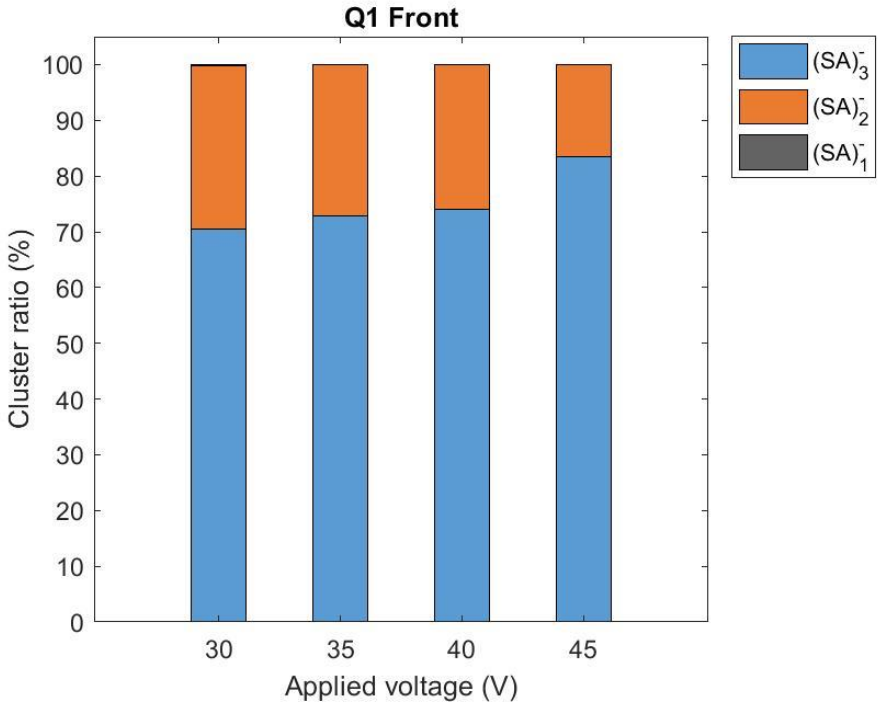

Figure S5. Percentage ratio of $(SA)_1^-$, $(SA)_2^-$ and $(SA)_3^-$ for different voltages applied to Q1 Front.

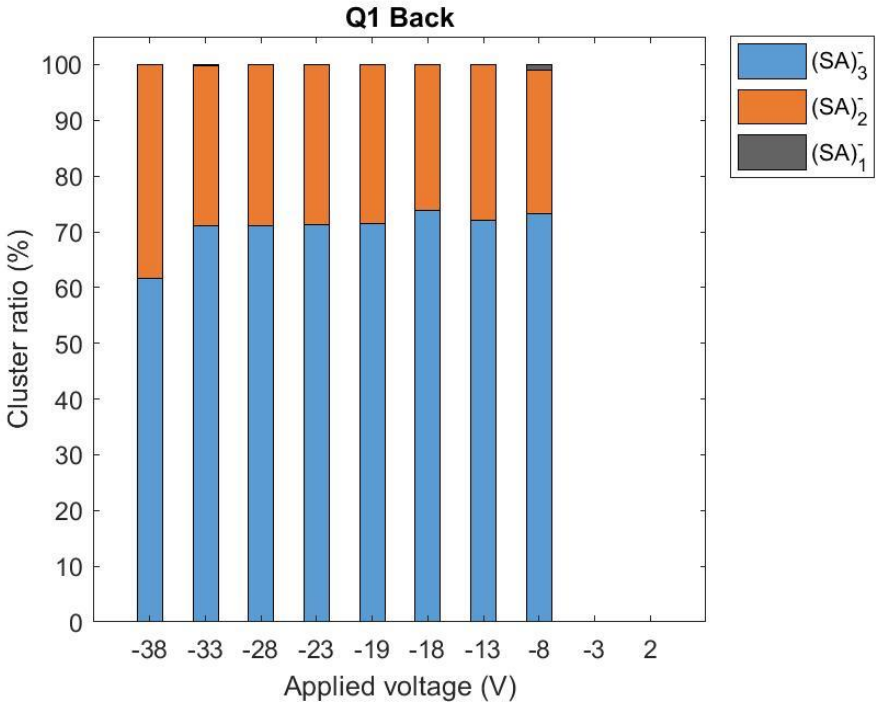

Figure S6. Percentage ratio of $(SA)_1^-$, $(SA)_2^-$ and $(SA)_3^-$ for different voltages applied to Q1 Back.

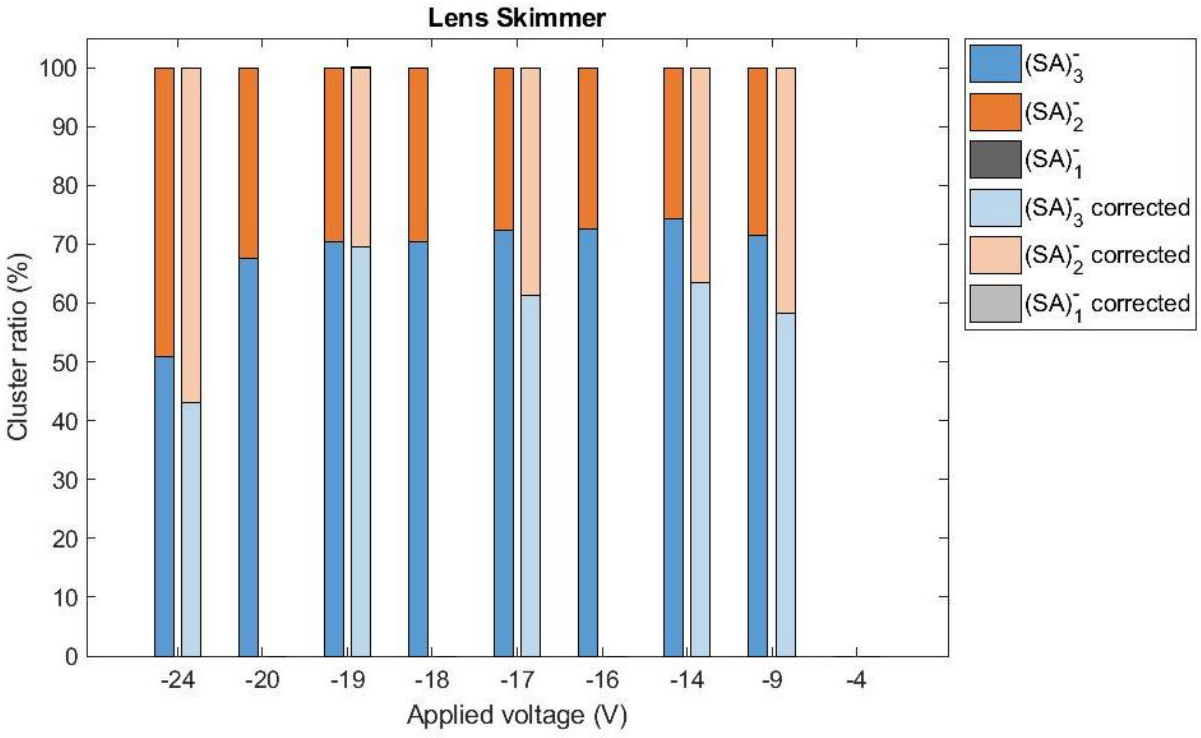

Figure S7. Percentage ratio of $(SA)_1^-$, $(SA)_2^-$ and $(SA)_3^-$ for different voltages applied to Lens Skimmer (darker colours). The ratios corrected by the transmission are reported in lighter colours.

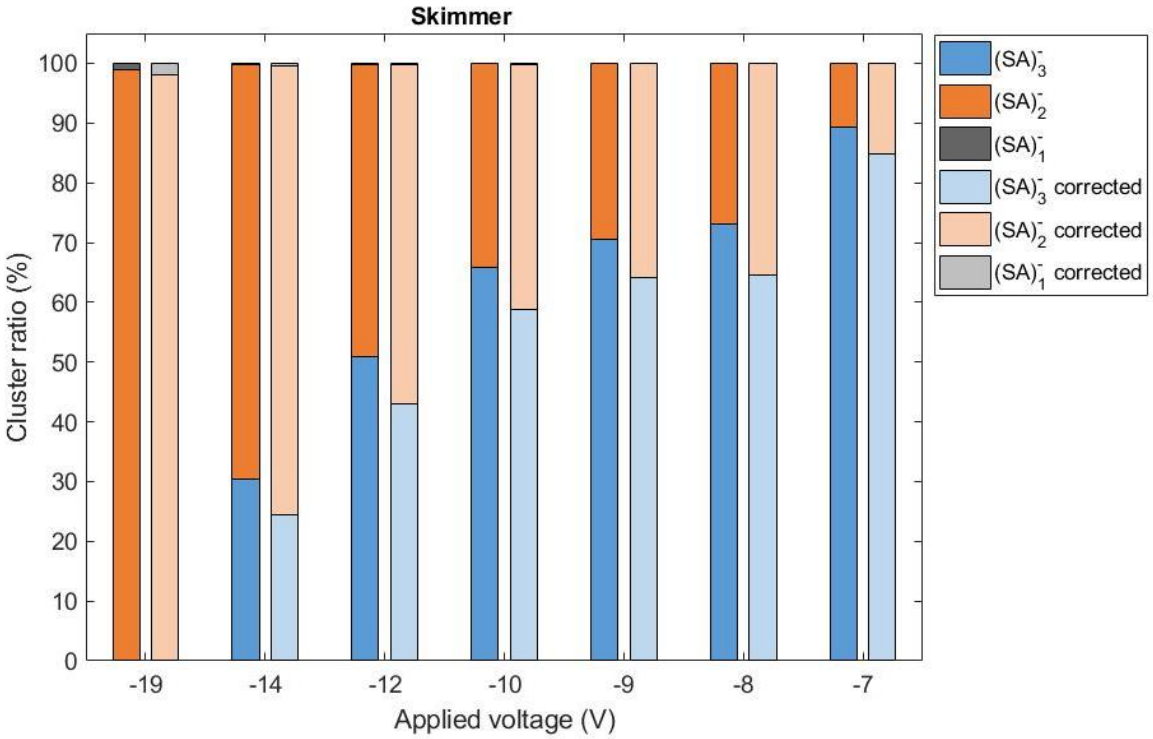

Figure S8. Percentage ratio of $(SA)_1^-$, $(SA)_2^-$ and $(SA)_3^-$ for different voltages applied to Skimmer (darker colours). The ratios corrected by the transmission are reported in lighter colours.

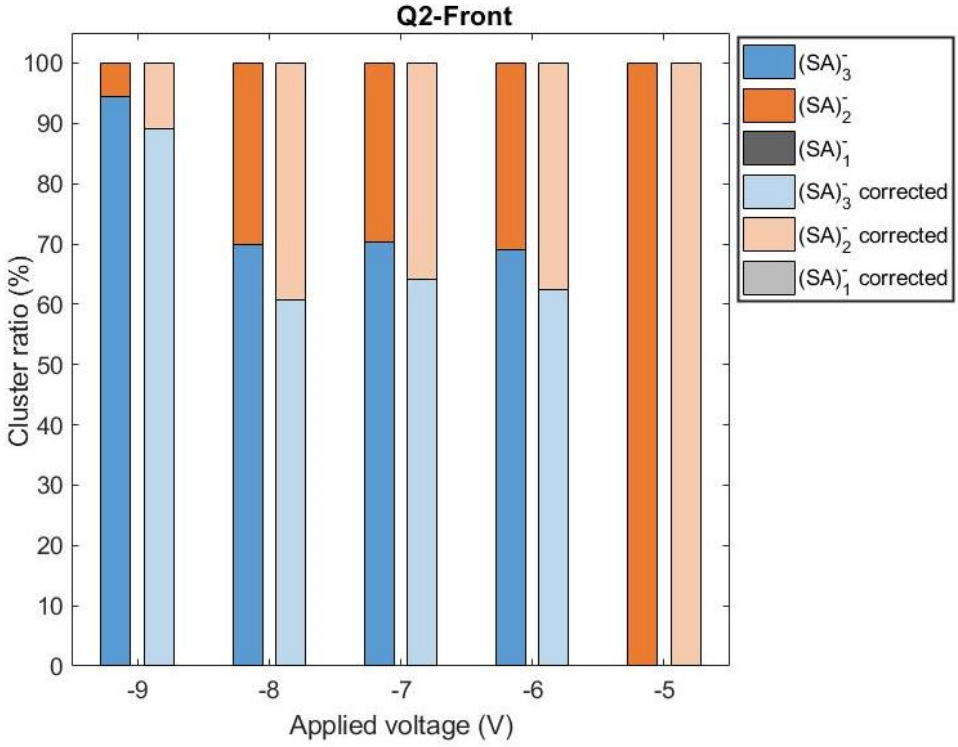

Figure S9. Percentage ratio of $(SA)_1^-$, $(SA)_2^-$ and $(SA)_3^-$ for different voltages applied to Q2 Front (darker colours). The ratios corrected by the transmission are reported in lighter colours.

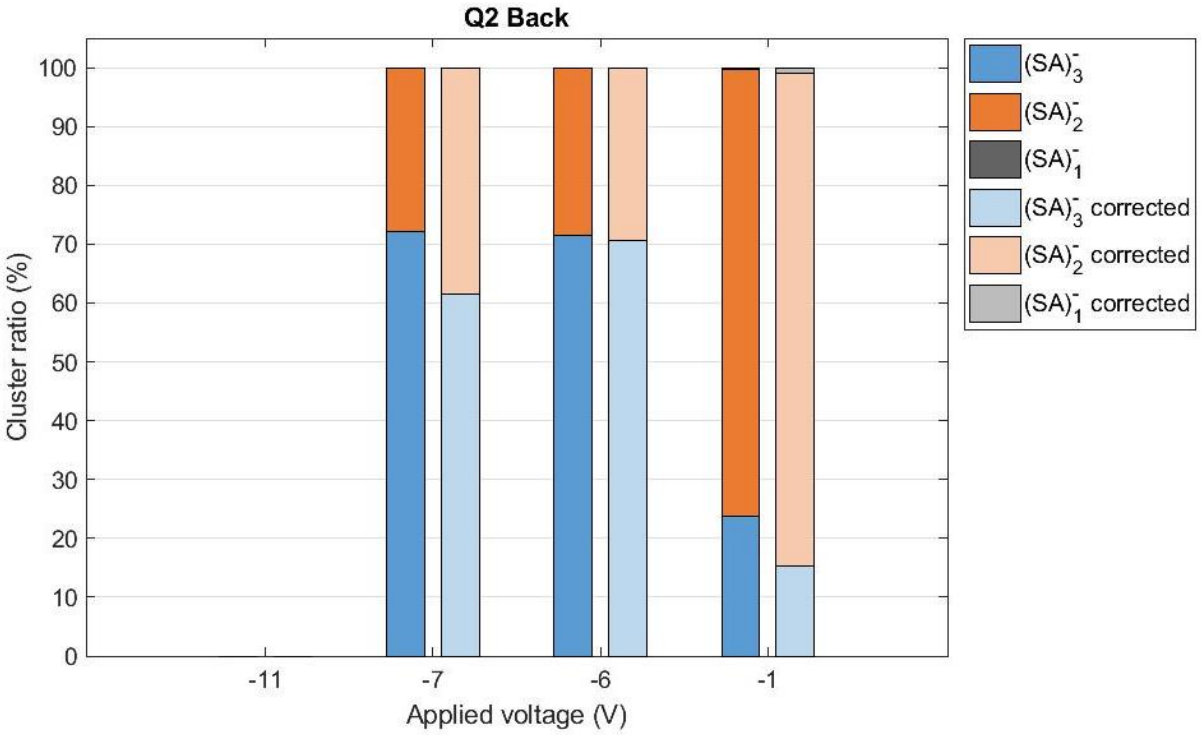

Figure S10. Percentage ratio of $(SA)_1^-$, $(SA)_2^-$ and $(SA)_3^-$ for different voltages applied to Q2 Back (darker colours). The ratios corrected by the transmission are reported in lighter colours.

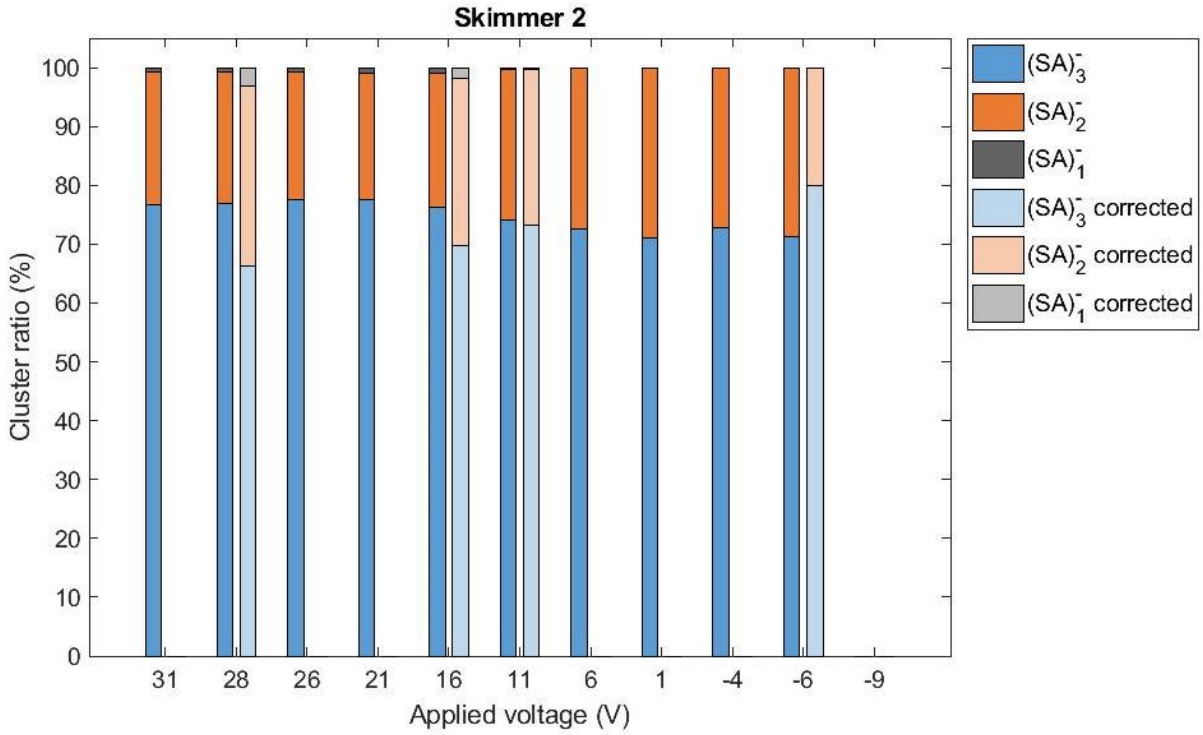

Figure S11. Percentage ratio of $(SA)_1^-$, $(SA)_2^-$ and $(SA)_3^-$ for different voltages applied to Skimmer 2 (darker colours). The ratios corrected by the transmission are reported in lighter colours.

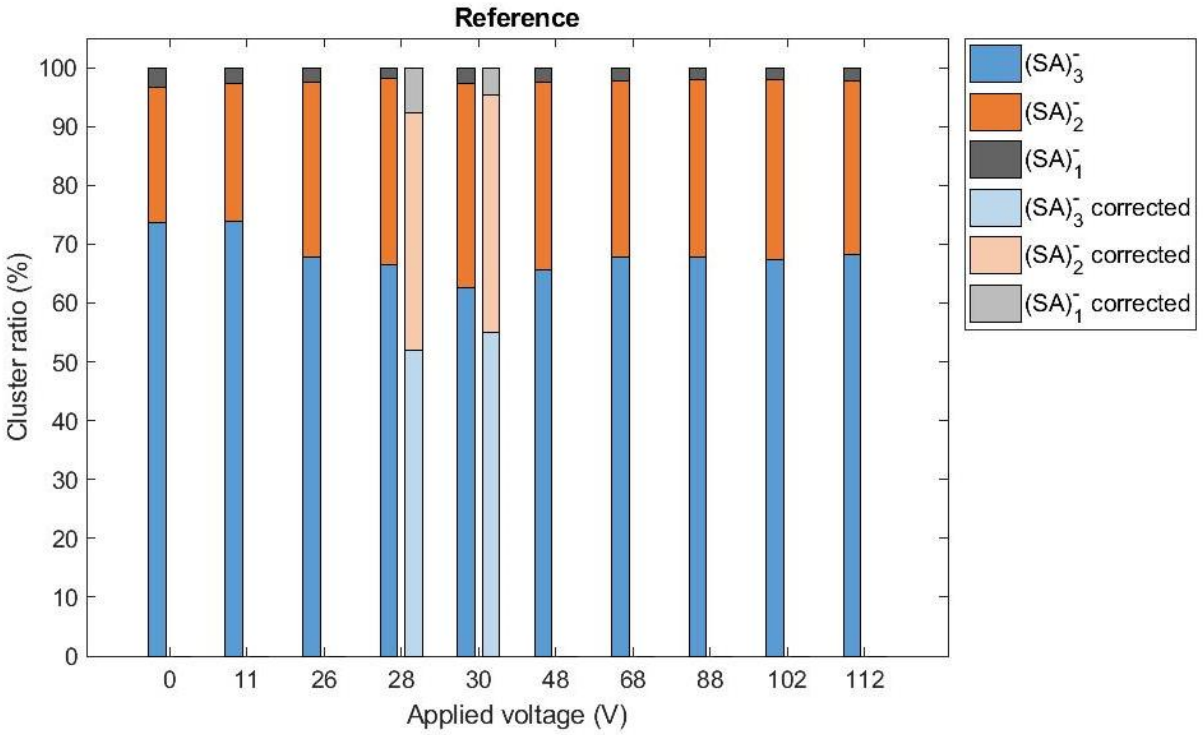

Figure S12. Percentage ratio of $(SA)_1^-$, $(SA)_2^-$ and $(SA)_3^-$ for different voltages applied to Reference (darker colours). The ratios corrected by the transmission are reported in lighter colours.

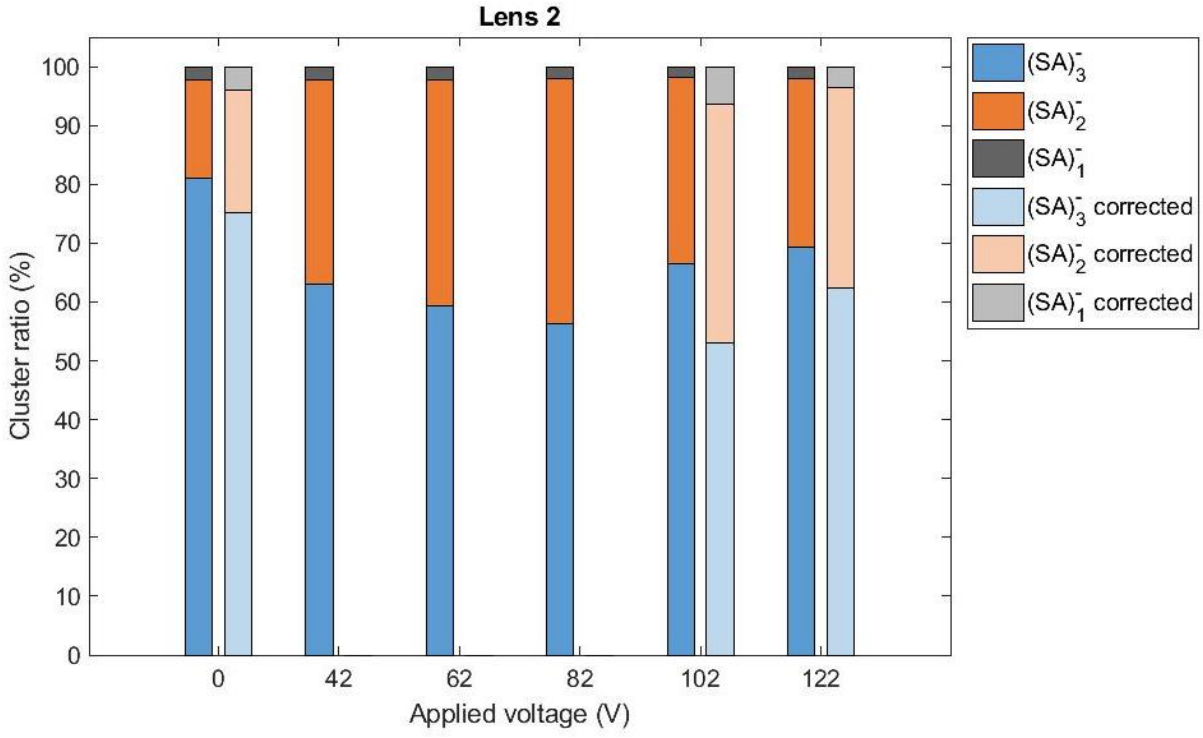

Figure S13. Percentage ratio of $(SA)_1^-$, $(SA)_2^-$ and $(SA)_3^-$ for different voltages applied to Lens 2 (darker colours). The ratios corrected by the transmission are reported in lighter colours.

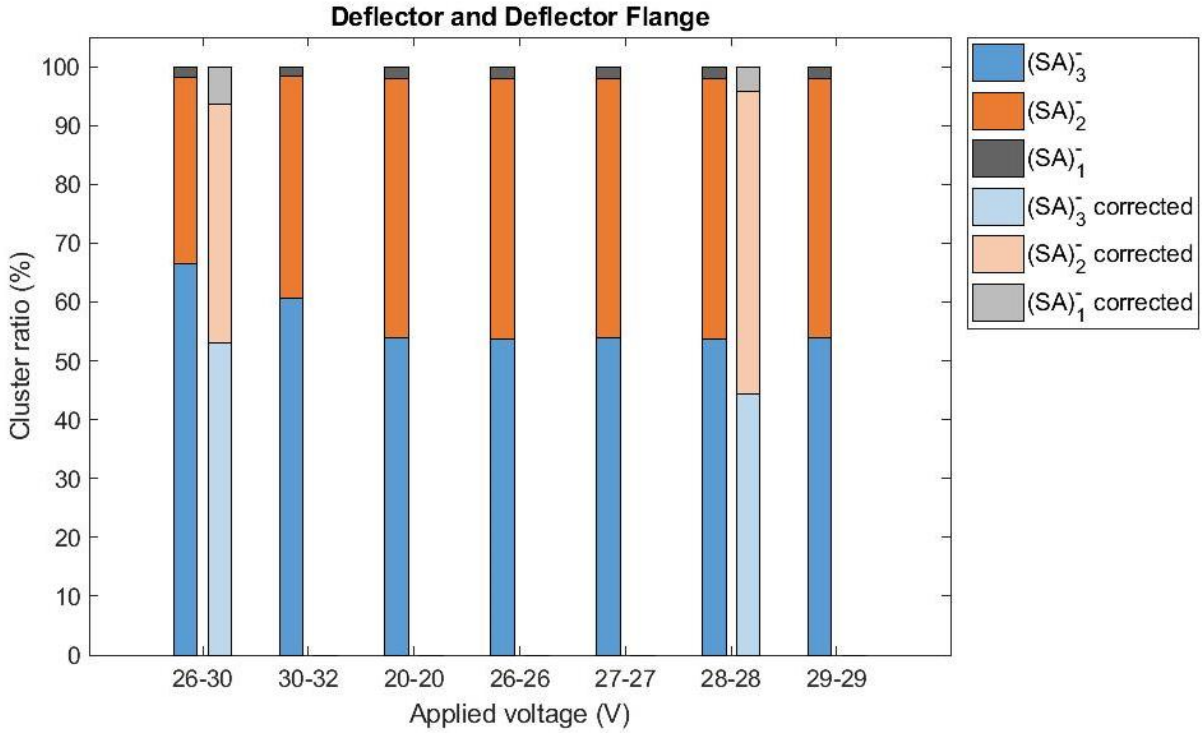

Figure S14. Percentage ratio of $(SA)_1^-$, $(SA)_2^-$ and $(SA)_3^-$ for different voltages applied to Deflector and Deflector Flange (darker colours). The ratios corrected by the transmission are reported in lighter colours.

4. Quantum chemistry calculations

There are three possible fragmentation pathways for the sulfuric acid trimer:

$(H_2SO_4)_2HSO_4^- \rightarrow H_2SO_4HSO_4^- + H_2SO_4$ (R1)

$(H_2SO_4)_2HSO_4^- \rightarrow HSO_4^- + 2\ H_2SO_4$ (R2)

$(H_2SO_4)_2HSO_4^- \rightarrow HSO_4^- + (H_2SO_4)_2$ (R3)

To define the most favourable fragmentation pathway of sulfuric acid trimer and the fragmentation rates used in our statistical model, we calculated zero point energy (ZPE) corrected fragmentation energies for pathways R1, R2, and R3. ZPE results from the vibrational motion of molecular systems even at 0 K and is calculated for a harmonic oscillator model as a sum of contributions from all vibrational modes of the system. All geometry optimizations and vibrational frequency calculations

were carried out in Gaussian 09 Rev. D.01.[6] Single point energy calculations were run using the Orca 4.0.1.2 program.[7] We used the semiempirically guided technique[8] to obtain the minimum energy structures for the clusters. First we created 200, 1000, and 2800 random cluster structures for $(SA)_2^-$, $(SA)_2$, and $(SA)_3^-$, respectively. The structures were subsequently optimized using the semiempirical PM6 method,[9] and all converged structures were then re-optimized at the DFT level PW91/6-31+G*.[10] The different structures were then characterized based on electronic energies and dipole moments, which were further optimized at the PW91/6-311++G** level of theory. Vibrational frequencies were also calculated at this level. Different conformations are sorted based on the ZPE-corrected electronic energies (E_0), and the final optimization and frequency calculation were performed at the PW91/aug-cc-pVQZ level of theory for one, four, and 22 lowest E_0 conformations of $(SA)_2^-$, $(SA)_2$, and $(SA)_3^-$ clusters, respectively. The electronic energy corrections are calculated on top of the DFT structures using DLPNO−CCSD(T)/aug-cc-pVTZ level of theory with a tight pair natural orbital criteria.[11] The lowest E_0 conformations at the DLPNO−CCSD(T)/aug-cc-pVTZ// PW91/aug-cc-pVQZ level are used to calculate ZPE-corrected fragmentation energies, which are for reaction (R1) 29.3 kcal/mol (Figure S15), reaction (R2) 76.4 kcal/mol and reaction (R3) 58.1 kcal/mol.

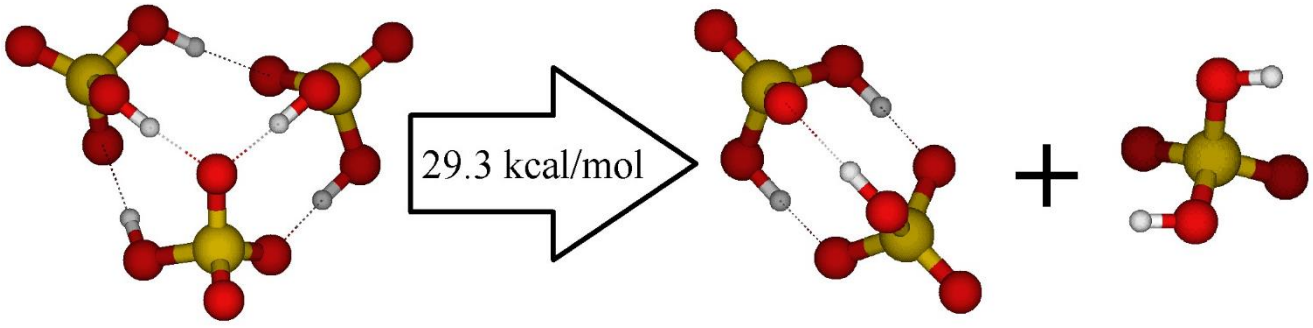

Figure S15. The fragmentation of $(SA)_3^-$ cluster to $(SA)_2^-$ and SA parts. Colour coding: yellow=sulfur, red=oxygen, and white=hydrogen.

5. Fragmentation rate constants and density of states

The ions are accelerated under the electrical field and collide with the carrier gas with velocities much higher than thermal velocities. As a consequence, the energy transferred to the internal modes of the ions also considerably differs from the thermal case. Therefore, to judge the fate of the ions inside the mass spectrometer, we cannot rely only on thermodynamic data. Instead, we need to know the fragmentation rate constant as a function of the energy of the ion rather than the temperature of the carrier gas. Note that the naive approach to relate the energy to temperature through ratios such as $E = kT$ (k is the Boltzmann constant) does not work, since computing a temperature-dependent rate constant requires that the energy of the ions obeys the Boltzmann distribution (which is not the case here).

In all unimolecular reaction theories, the key value defining the rate constant is the ratio of the combined density of states of the products to the density of states of the reactant. The pre-factor to this ratio differs from theory to theory. To calculate it we have used the detailed balance approach and the recipe to take into account conservation of the momentum and angular momentum developed in the paper by Zapadinsky et al.[12] All computational details can be found there.

The densities of states have been calculated with the frequencies and rotational constants obtained for minimum energy conformers. The fragmentation energies have been calculated using electronic energies for the products and reactants corrected with zero-point energy value. The quantum chemical methods are the same as in the previous section.

The fragmentation rate constants of $(SA)_3^-$ for all possible channels are presented in Figure S16. The fragmentation rate constants reported in Figure S16 have been derived from quantum chemistry data calculated at the PW91/aug-cc-pVQZ level of theory.

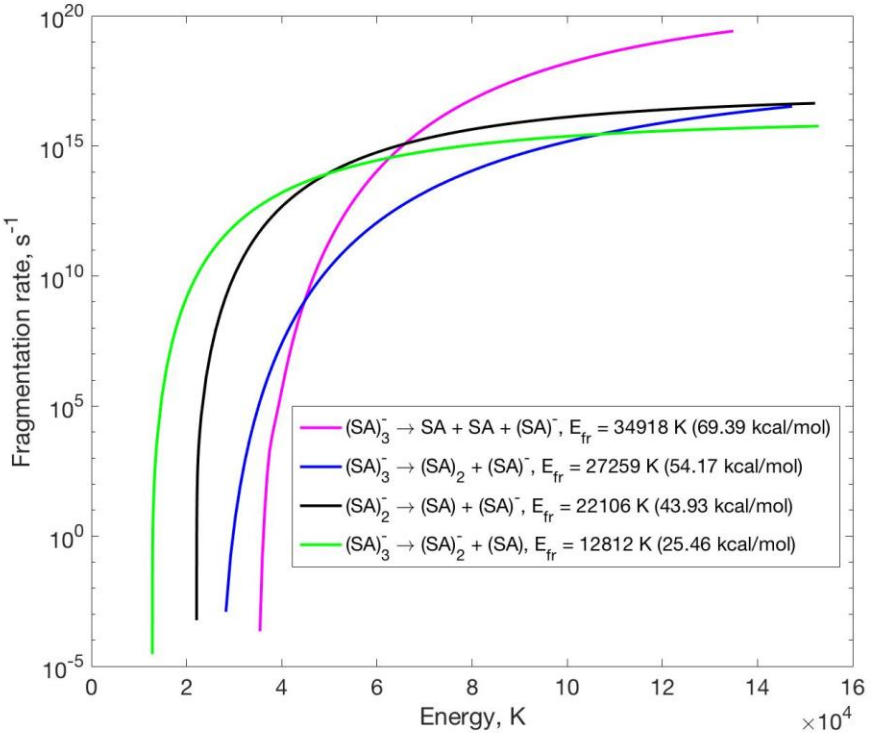

Figure S16. The fragmentation rate constants of $(SA)_3^-$ and $(SA)_2^-$ for all pathways.

Based on the rate constants, we can conclude that the only possible pathway for fragmentation of the trimer is R1. Other channels are completely negligible at times between the collisions with the carrier gas and for typical energy transfers occurring during one collision in the conditions of the experiment. The charged sulfuric acid monomers can be observed in the experiment only due to the secondary process following the pathway R1. The energies necessary for the fragmentation of $(SA)_2^-$ are reachable in the experiment. The fragmentation rate constant of $(SA)_2^-$ is also presented in Figure S16.

6. Short description of the model

Our model describes the ion's trajectory through the APi, and the collisions between the ion and the carrier gas molecules. During the collision, energy is transferred to the cluster, which can then fragment due to the excess of energy. In our model, we consider the trajectory and the fate of each ion as an individual run, which we call a realization. The ion moves under the electric field, and experiences collisions with the carrier gas.

To simulate the trajectory of clusters inside the quadrupole we consider that the ion moves only under the electric field defined by the voltages applied to the beginning and to the end of the quadrupole. We modelled the effect of the alternating voltage applied to the quadrupole on the cluster fragmentation, and observed that the effect is negligible. The main effect of the applied radiofrequencies is to decrease the velocities of the clusters in the transverse directions, and to focus them along the main axis chamber. Since the transverse velocity is much less than the velocity along the main axis, its contribution to the probability of collision is negligible. Hence the probability of fragmentation is also not affected.

The collision frequency between carrier gas molecules and clusters is governed by the probability density function (PDF) depending on the density and temperature of the carrier gas and the velocity of the ion. At the collision, the translational energy can be transferred to rotational and vibrational energy of the ion. The amount of transferred energy is defined by PDFs calculated on the basis of the conservation laws (energy, momentum and angular momentum), microcanonical ensemble principle and the vibrational density of states of the ion. The conservation laws are considered separately for the normal and tangential (with respect to the ion) components of the velocity of the carrier gas. Under the term microcanonical ensemble principle, we imply that all microstates having the same energy occur with equal probability. The normal component transfers energy to the vibrational and translational modes of the ion, while the tangential component transfers energy to the rotational and

translational modes. The amount of energy transferred to the vibrational modes of the ion is defined by the vibrational density of states. The amount of energy transferred to the rotational modes of the ion is defined by the conservation laws.

After the collision, there is an exchange energy between the vibrational and rotational modes of the ion. This process is governed by a PDF defined by the vibrational and rotational densities of states. In the period between the collisions, there is a chance for the fragmentation of the ion. The probability of fragmentation is governed by a PDF defined by the fragmentation rate constant.

All computational details can be found in the paper by Zapadinsky et al.[12]

The simulation process can be divided in 6 steps (Scheme S1):

1. Initial settings of the all modes of the cluster. For rotational and vibrational modes, we have used random values taken from the Boltzmann distribution at 300 K. For the translational modes, we used either fixed values or random velocities from the Maxwell distribution at 300 K. For both cases we had identical fragmentation rates.
2. The cluster moves in the electric field. From an appropriate probability density function (PDF), depending on the carrier gas density, temperature and velocity of the cluster, a time of the next collision with a carrier gas molecule is defined.
3. Check if fragmentation occurs before the next collision, or before the ion reaches the end of the simulated region. The fragmentation PDF is defined by the rate constant depending on the cluster energy. There are three possibilities:
   - the ion reaches the end of the simulated region, the cluster is counted as survived, and a new cluster trajectory (realization) is started.
   - if fragmentation occurs, the cluster is counted as fragmented, and a new cluster trajectory (realization) is started.
   - if fragmentation does not occur, the simulation continues with step 4.

4. A random collision point at the cluster surface and direction is assigned for the carrier gas molecule collision. The point and direction of the collision follow an appropriate PDF as the cluster is moving in a certain direction relative to the carrier gas.
5. At the collision, the translational energy of the carrier gas molecule is transferred to rotational and vibrational energy of the ion.
6. The energy is redistributed among rotational and vibrational energy modes according to the conservation laws, and a PDF defined by the density of states. The simulation continues from step 2 until fragmentation occurs, or until the cluster reaches the end of the modelled region.

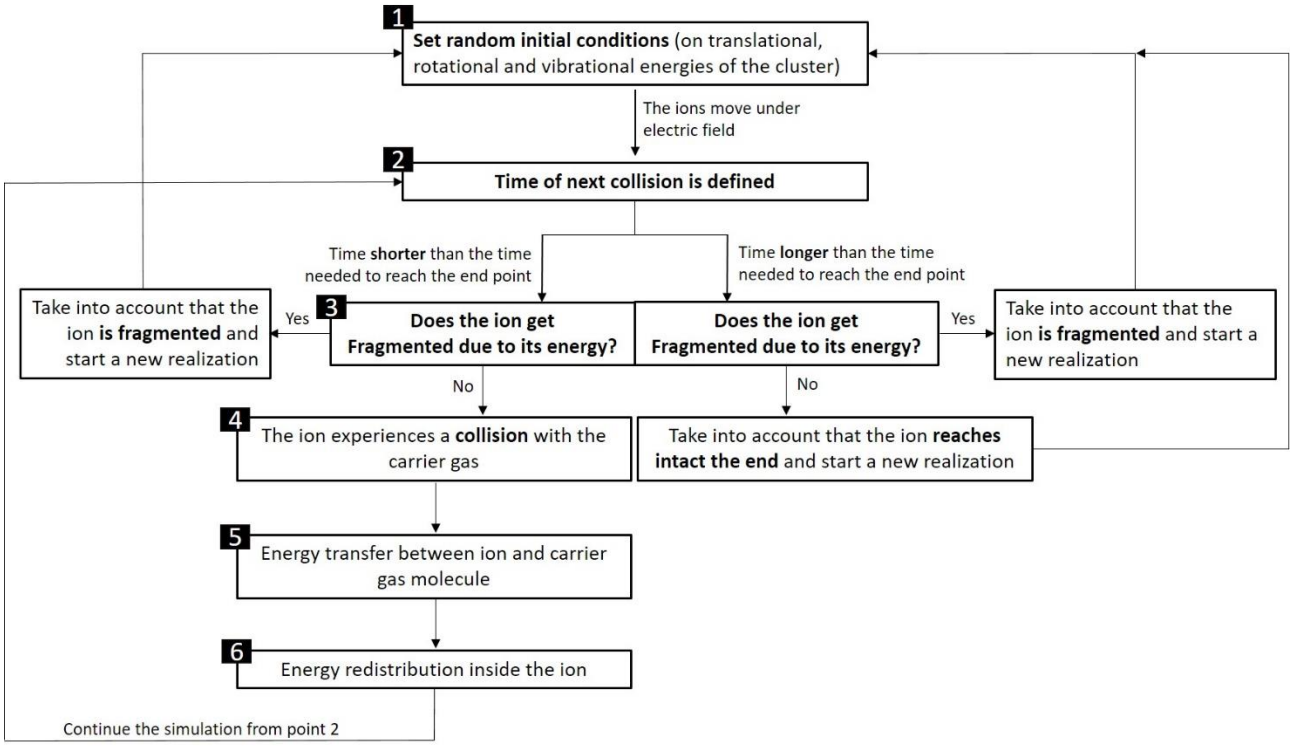

Scheme S1. Flow chart of the simulation.

7. Effect of carrier gas properties

In our simulations, we used air as carrier gas and we defined the properties of the carrier gas as an average between N_2 and O_2, according to the relative abundance in the atmosphere. More details about the carrier gas properties are reported in Zapadinsky et al.[12] It is important to notice that we neglect the effect of long-range interaction on the collision frequency due to the low polarizability of N_2 and O_2.[13] Also in case of noble gases (e.g. argon, helium) as carrier gas, as often used in other MS analysis, this assumption is valid.

One of the properties of the carrier gas that can significantly affect the fragmentation is the cross section. We have simulated the fragmentation of sulfuric acid trimer negatively charged using different collision radius to evaluate the effect of the collision cross section on cluster fragmentation. The results of the simulations are reported in figures S17 and S18.

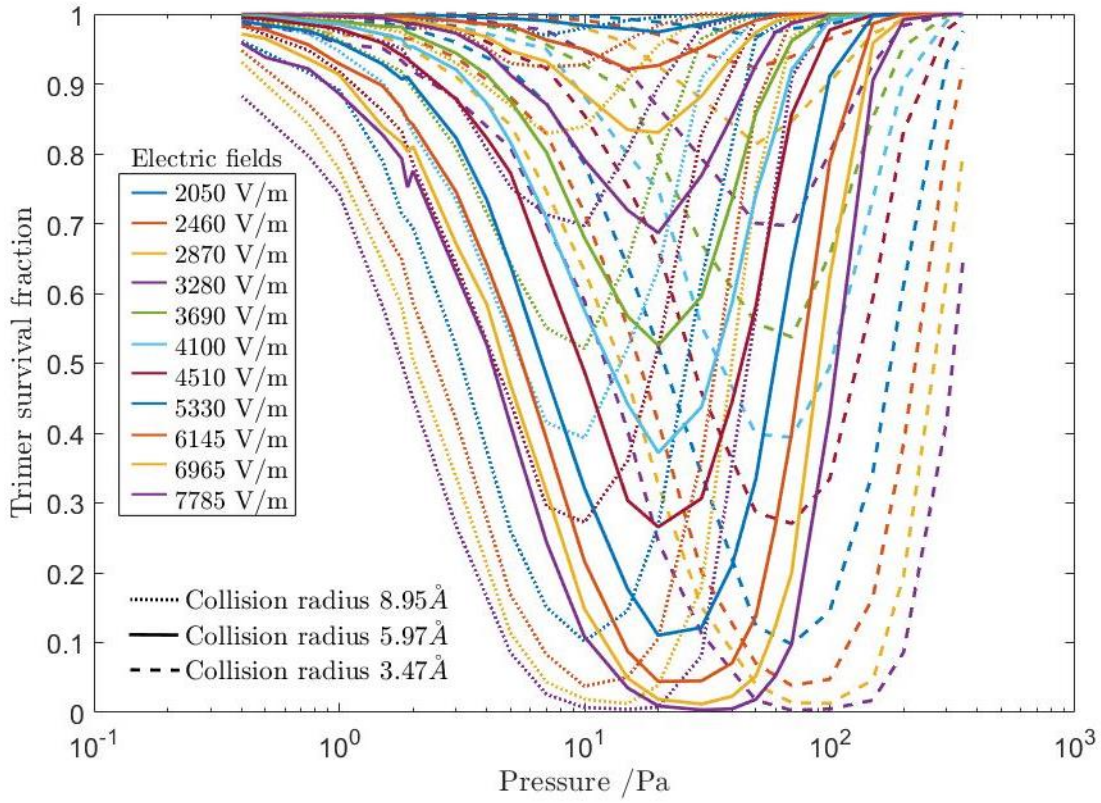

Figure S17. Dependence of the sulfuric acid trimer $(SA)_3^-$ fragmentation on pressure at different values of electric field and collision radius.

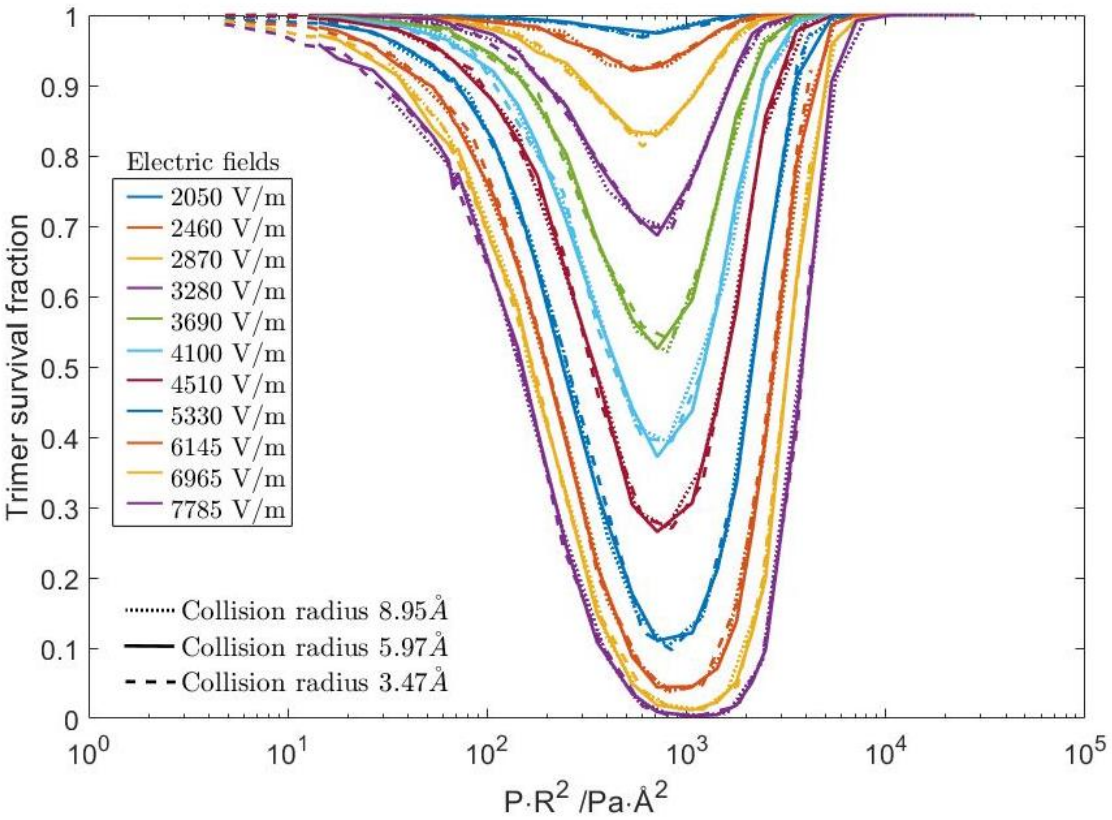

Figure S18. Dependence of the sulfuric acid trimer $(SA)_3^-$ fragmentation on pressure (P) and collision radius (R) at different values of electric field.

Figures 17 and 18 show the results of the same simulations at different pressures, collision radii and electric fields. We can see that if the trimer survival fraction is plotted versus the product of pressure and collision radius in the second power, all curves with the same electric field merge into one.

8. Modelling the pressure inside the APi

The measured pressure corresponds to the area where the pressure sensor is connected, roughly in the middle of the chambers. However, for accurate modelling of the cluster fragmentation we need to know the density and temperature of the carrier gas also near and inside the skimmers connecting the chambers. The diameter of the skimmer orifice between the first and second chambers is much greater

than the mean free path at the end of the first chamber. Therefore, we have considered the outgoing flow from the first chamber as continuous. The velocity of the flux, pressure, density and temperature inside the skimmer have been calculated using the Bernoulli principle, adiabatic expansion and continuity equations. Right after the end of the skimmer, at the beginning of the second chamber, the pressure, density and temperature reach, within the length of the mean free path the conditions of the second chamber. According to the heat and mass balance calculations the temperature of the second chamber far from the orifices is close to room temperature.

The accurate calculation of the fluid dynamics factors in the interface between the first and second chambers requires considerable efforts. Before undertaking this problem, we have varied in the model the dimensions of the skimmer. We have seen changes up to 7% in the degree of cluster fragmentation. However, these changes are not dramatic enough to affect our main conclusions. Therefore, we have postponed the detailed study of the fluid dynamics in the interface between the first and the second chambers.

The diameter of the orifice of the skimmer between the second and the third chambers is less than the mean free path in this area. Therefore, for the calculation of the collision PDF near the skimmer to the third chamber, we assume that there are no carrier gas molecules coming from the orifice area that the cluster can collide with.

9. Uncertainties evaluation of the simulations

The sources of uncertainties in our model can be divided into three groups. The first group is related to the physical principles involved in the simulation, especially the details of the energy transfer at collisions. The second group is corresponds to the calculated parameters of the cluster. The third group is connected to our incomplete knowledge of the simulated system.

353 Thorough evaluation of the first group is outside of the scope of the present study. We just mention
354 here the crucial role that conservation laws play in the energy transfer process. Also, our energy
355 transfer model assumes that there are no obstacles for energy flow to the internal modes of the cluster,
356 as long as the energy levels are available. This principle leads to maximal possible energy transfer to
357 the cluster internal modes at collisions. The validity of these assumptions can be checked by
358 molecular dynamics simulations.

359 The cluster parameters such as density of states and radius are calculated by quantum chemistry using
360 rigid-rotor-harmonic approximation. It has been widely discussed that this approximation works
361 relatively well, despite the obvious errors introduced by rotational-vibrational coupling,
362 anharmonicity of the vibrations and treatment of the lowest modes as vibrations. The role of the
363 quantum chemistry method is significant. We have compared fragmentation energies calculated by
364 two methods: DFT level PW91/aug-cc-pVQZ and DLPNO−CCSD(T)/aug-cc-pVTZ// PW91/aug-cc-
365 pVQZ level of theory with a tight pair natural orbital criteria. The first method gives 25.46 kcal/mol
366 while the second, more accurate method gives 29.3 kcal/mol. We have run simulations at conditions
367 of the Cases A and B (see the main text) for the fragmentation rate constant based on these two
368 methods. As we can see from Figure S19, the more accurate quantum chemistry method produces
369 results closer to the experimental data, however, the DFT-based method also performs reasonably
370 well.

371 The uncertainty in the fluid dynamics has been already discussed in the previous section. Another
372 example of the incomplete knowledge is the shape of electrodes. It is unknown to us and we assumed
373 that electric field due to them is as they were the infinite plates like in a flat capacitor. Obviously, the
374 electrodes have holes for passing of the ions. We have estimated how possible corrections to the
375 electric fields due to the edge effects can change the degree of the cluster fragmentation. Variation of
376 the electric field when the ion passes through electrode from zero to the one equal to the electric field
377 from the infinite plate has shown the possible effect on the level of the cluster fragmentation to be

about 25%. For the Figure 5 of the main text we have used averages over these two extreme cases for the electric field.

We see that for accurate modelling of the experimental results on the cluster fragmentation inside the mass spectrometer, one needs detailed knowledge of the system, and thorough methods for calculation of the cluster parameters. However, the results of the present study allow us to conclude that even with incomplete knowledge of the system, the effect of the cluster fragmentation on the results of the mass spectrometer measurements can be estimated relatively well.

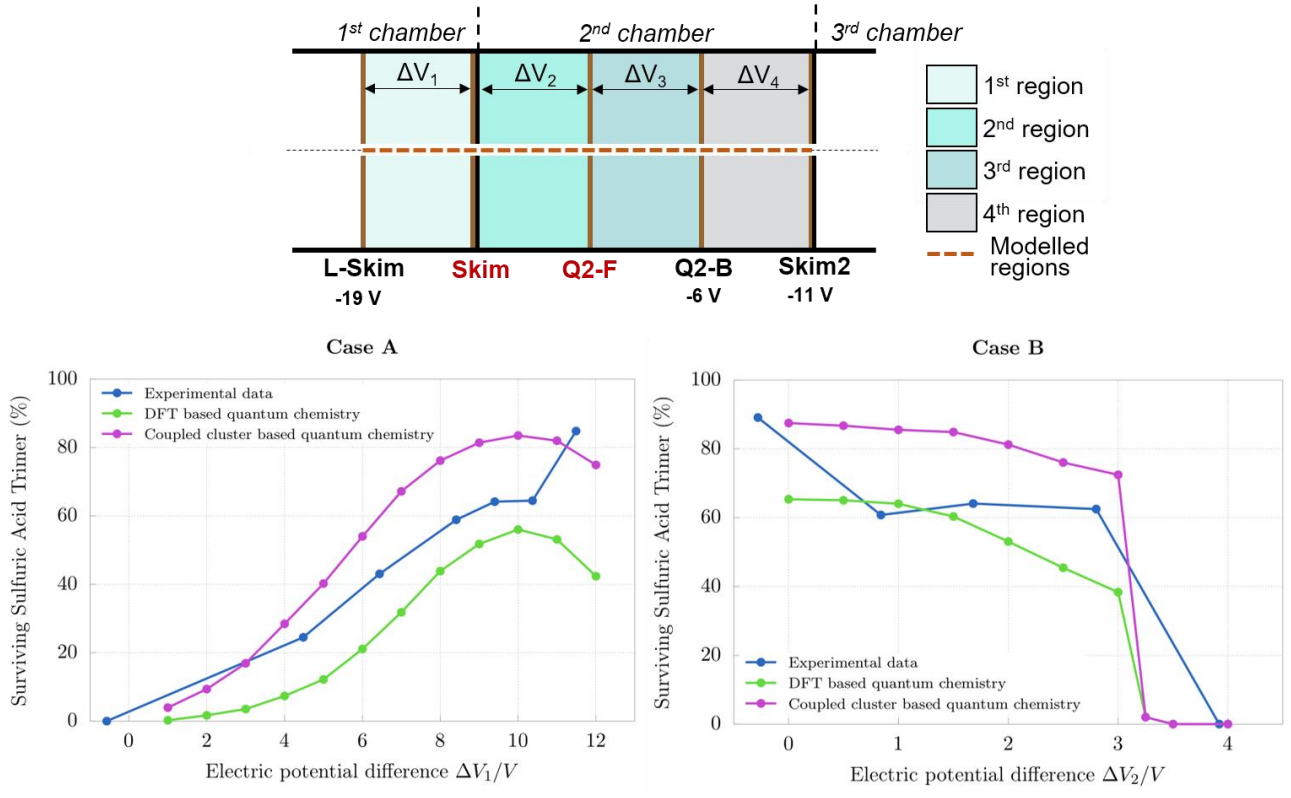

Figure S19. Comparison of the simulation results performed with two different fragmentation rate constants based on two quantum chemical methods. In the upper panel a schematic representation of the region between Lens Skimmer and Skimmer2. The lower panel shows the experimental and modelled $R_{(SA)_3}$ as a function of the electric potential difference between to electrodes (ΔV). In the graph A the experimental and modelled $R_{(SA)_3^-}$ is reported as a function of ΔV_1. During these experiments and corresponding simulations only the voltages applied to the Skimmer were changed.

In the graph B the experimental and modelled $R_{(SA)_3^-}$ is reported as a function of ΔV_2. During these experiments and simulations only the voltages applied to the Q2-Front were changed.

10.References

[1] a) F. Bianchi et al., *Environ. Sci. Technol.* **2014**, *48*, 13675-13684; b) T. Jokinen, M. Sipilä, H. Junninen, M. Ehn, G. Lönn, J. Hakala, T. Petäjä, R. L. Mauldin III, M. Kulmala, D. R. Worsnop, *Atmos. Chem. Phys.* **2012**, *12*, 4117-4125; c) A. Kürten, L. Rondo, S. Ehrhart, J. Curtius, *Atmos. Meas. Tech.* **2011**, *4*, 437-443.

[2] J. Kangasluoma, M. Attoui, F. Korhonen, L. Ahonen, E. Siivola, T. Petäjä, *Aerosol Sci. Technol.* **2016**, *50*, 222-229.

[3] H. Junninen et al., *Atmos. Meas. Tech.* **2010**, *3*, 1039-1053.

[4] F. D. Lopez-Hilfiker, S. Iyer, C. Mohr, B. H. Lee, E. L. D'Ambro, T. Kurtén, J. A. Thornton, *Atmos. Meas. Tech.* **2016**, *9*, 1505-1512.

[5] M. Heinritzi, M. Simon, G. Steiner, A. C. Wagner, A. Kürten, A. Hansel, J. Curtius, *Atmos. Meas. Tech.* **2016**, *9*, 1449-1460.

[6] M. J. Frisch et al., *Gaussian 16* **2016**, *revision A.03; Gaussian, Inc.: Wallingford, CT*

[7] F. Neese, *Wiley Interdiscip. Rev. Comput. Mol. Sci.* **2012**, *2*, 73-78.

[8] J. Elm, M. Bilde, K. V. Mikkelsen, *J. Phys. Chem. A* **2013**, *117*, 6695-6701.

[9] J. J. P. Stewart, *J. Mol. Model.* **2007**, *13*, 1173-1213.

[10] J. P. Perdew, Y. Wang, *Phys. Rev. B: Condens. Matter Mater. Phys.* **1992**, *45*, 13244-13249.

[11] a) N. Myllys, J. Elm, R. Halonen, T. Kurtén, H. Vehkamäki, *J. Phys. Chem. A* **2016**, *120*, 621-630; b) C. Riplinger, P. Pinski, U. Becker, E. F. Valeev, F. Neese, *J. Chem. Phys.* **2016**, *144*, 024109.

[12] E. Zapadinsky, M. Passananti, N. Myllys, T. Kurtén, H. Vehkamäki, *J. Phys. Chem. A* **2019**, *123*, 611-624.

[13] D. Spelsberg, W. Meyer, *J. Chem. Phys.* **1994**, *101*, 1282-1288.